NANO LETTERS

pubs.acs.org/NanoLett Letter

Visualizing the Orientation of Single Polymers Induced by Spin-Coating

Jonathan M. Chan and Muzhou Wang*

Cite This: https://doi.org/10.1021/acs.nanolett.2c01830 Read Online

ACCESS | Metrics & More | Article Recommendations | Supporting Information

ABSTRACT: The orientation of chains within polymeric materials influences their electrical, mechanical, and thermal properties. While many techniques can infer the orientation distribution of a bulk ensemble, it is challenging to determine this information at the single-chain level, particularly in an environment of otherwise identical polymers. Here, we use single-molecule localization microscopy (SMLM) to visualize the directions of chains within spin-coated polymer films. We find a strong relationship between shear force and the degree and direction of orientation, and additionally, we reveal the effects of chain length and solvent evaporation rate. This work utilizes single-chain resolution to observe the important, though often overlooked, property of chain orientation in the common fabrication process of spin-coating.

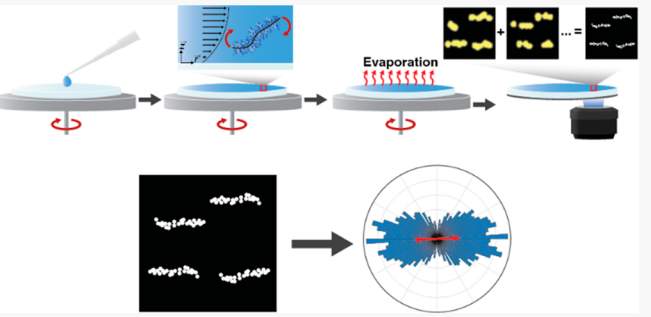

KEYWORDS: *bottlebrush polymer, super-resolution microscopy, spin-coating, orientation*

Spin coating is a universal process used to prepare thin polymer films with uniform thickness. Researchers have observed anisotropic distributions in orientations of polymer chains as a result of spin-coating,[1] which has potential implications for improving electron transport,[2−6] mechanical strength,[7−9] and thermal conductivity.[10,11] While techniques such as Fourier transformed infrared (FTIR) microscopy,[12] birefringence,[13,14] and polarized resonant soft X-ray scattering (P-RSoXS)[15,16] have inferred chain orientation within polymeric materials by probing bulk environments and fitting data to models, they lack the specificity of studying individual molecules. Single-chain specificity is especially useful in studying orientation around defects in bulk polymeric materials, where fractures propagated by defects can additionally be affected by the orientation of chains.[17,18] In another example, liquid crystals derive optical properties from the order of their molecules, and defects within this system disrupt order as the chains orient themselves around these features.[19] So far, a deficit in single-chain and regional specificity prevents a deeper understanding of orientation-driven properties and functions.

Bottlebrush polymers are one notable example where orientation plays a significant role. For example, spun-coat bottlebrush films have displayed strongly oriented features with little processing due to their conformational rigidity.[20] Orientation is particularly valuable in bottlebrush block copolymer systems, where their well-ordered, highly oriented self-assembled features are desired for photonic materials and nanolithography.[21−24] In the example of lamellae-forming ABC bottlebrush triblocks, P-RSoXS has suggested that chains are not as rigid and ordered as intuitively expected, but rather, these chains experience a high degree of looping between lamellae.[25] Another study using self-consistent field theory and small-angle X-ray scattering (SAXS) of AB bottlebrush diblocks has implied high degrees of orientation at domain interfaces, but this orientation decreases toward the domain centers.[26] These cases are just some examples of where orientation strongly depends on the location within the system, requiring a technique that provides locally specific information at the single-chain level.

One technique that achieves such high resolutions and specificity is super-resolution optical microscopy.[27,28] This technique possesses resolutions of tens of nanometers and uses strategic fluorescent-labeling schemes that can provide images of individual polymers within a matrix of otherwise chemically identical species. In past studies, single-molecule localization microscopy (SMLM) was used to image bottlebrush polymers within a densely occupied polymer environment.[29] While this previous study has provided considerable insight into the static properties of bottlebrushes in equilibrium, single-polymer imaging in bulk environments under flow and far from equilibrium has yet to be realized.

Received: May 5, 2022
Revised: June 28, 2022

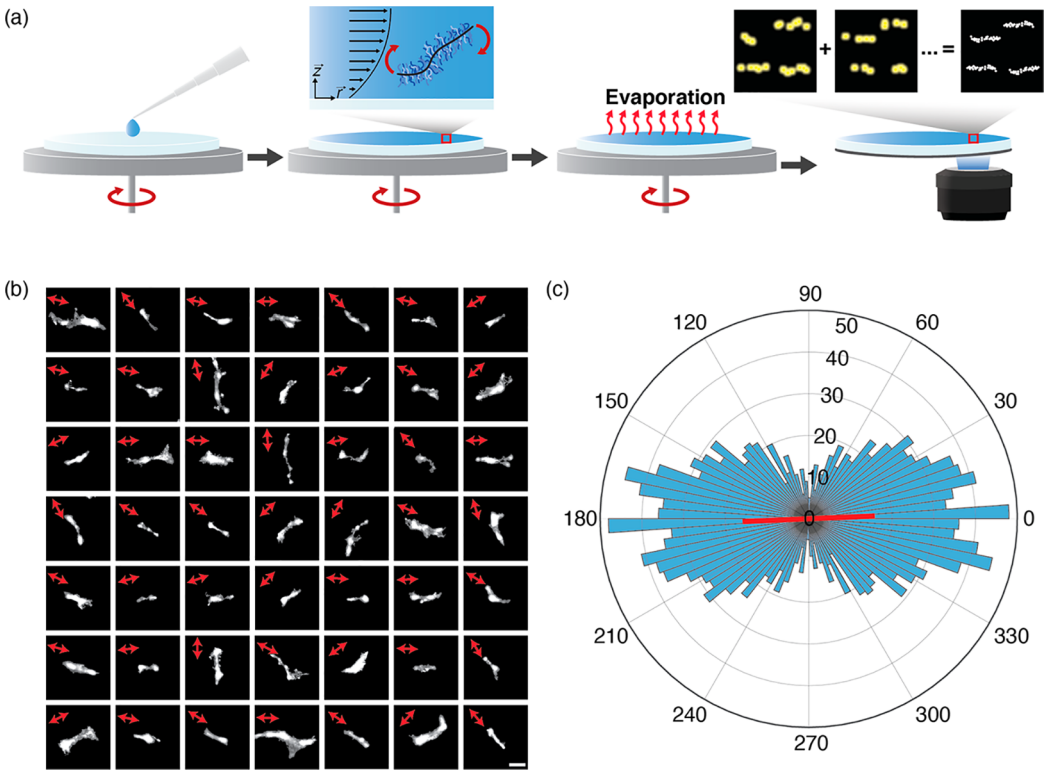

Figure 1. (a) Schematic describing spin-coating of polymer films and imaging by super-resolution microscopy. As a polymer solution is deposited on the spinning substrate, the fluid undergoes a two-step process: (1) a step dominated by an outward flow induced by centrifugal forces and (2) a step dominated by evaporation of solvent from the film. Following these steps, the orientations of the immobile chains can be directly observed using super-resolution microscopy. (b) A mosaic of 49 randomly chosen super-resolution images of bottlebrush polymer chains within a linear PMMA matrix spun from toluene. Red arrows indicate the direction of the end-to-end vector. The scale bar is 200 nm in length, and all images are the same magnification. The film thickness is 40 nm, and the images were acquired 5 mm to the right of the center of the coverslip. (c) The orientations of the end-to-end vectors of 1068 imaged chains are plotted in the polar histogram, with angular bins of 4° in width. The order parameter is $S = 0.32$. The red line points in the direction of the average orientation of the ensemble, and the ratio of its length to the diameter of the circle indicates the value of the order parameter.

SMLM offers an excellent opportunity to operate in bulk environments while providing the level of detail achieved using single-polymer rheology experiments. These studies have previously shown images of single-polymer chains in flow but are typically limited to large biopolymers such as DNA or actin and only in relatively dilute solution conditions. For bottlebrush polymers, many properties in response to flow in the bulk are highly relevant for numerous applications.[30,31] For example, effects of shear flow play an immediate influence on a tunable color 3D printing platform that uses bottlebrush polymers as the ink.[32] Additionally, researchers have found that these materials exhibit characteristic strain hardening under certain flow conditions, which affect their behavior during melt extrusion and printing.[33] Further study of bottlebrushes in flow by SMLM can also provide fundamental insight into the rheology of rigid or semiflexible polymers, which encompasses a wide category of materials.[34−36]

In this Letter, we show that bottlebrush polymers orient in the direction of the centrifugal force induced by spin-coating. Using super-resolution microscopy, we image individual polymer chains and analyze the orientations of ensembles of chains at various locations in the polymer films. To further study the variability of these orientations, the effect of evaporation rate is also studied by changing solvents used for spin-coating. We further investigate the features relevant to these orientation effects by probing effects of chain length and rigidity. Ultimately, SMLM reveals the orientation of single-polymer chains within a spun coat film, a feat that is difficult to achieve using other techniques.

To visualize the orientation distributions of single polymers after spin-coating, we synthesized fluorescently labeled bottlebrush polymers, imaged spun-coat thin films using SMLM, and then analyzed their end-to-end vectors. We used bottlebrush polymers consisting of a poly(hydroxyl-ethyl methacrylate) (PHEMA) backbone with poly(methyl methacrylate) (PMMA) side chains synthesized and fluorescently labeled using previously reported methods.[29] The bottlebrush polymers have $DP_{n,bb} = 3150$ and side chains with $M_n = 6500$ g/mol and $Đ = 1.3$. Films of 40 nm thickness were prepared by spin-coating a polymer solution of linear PMMA (M_n = 350 000 g/mol) with a dilute amount of the labeled bottlebrushes onto coverslips. Figure 1b shows SMLM images of 49 randomly chosen bottlebrushes imaged 5 mm from the center of the coverslip. The orientations of the end-to-end vectors for an ensemble composed of 1068 chains were plotted on a polar histogram (Figure 1c). From this histogram, the chains appeared to be oriented in the same general direction. We also found that the directionality of the chains disappears when the chains were given the opportunity to relax by thermal annealing (Figures S3 and S4).

We confirmed the significance of the perceived orientation of the end-to-end vectors of the polymer chains by performing a Rayleigh test for angular uniformity, against a null hypothesis

https://doi.org/10.1021/acs.nanolett.2c01830
Nano Lett. XXXX, XXX, XXX−XXX

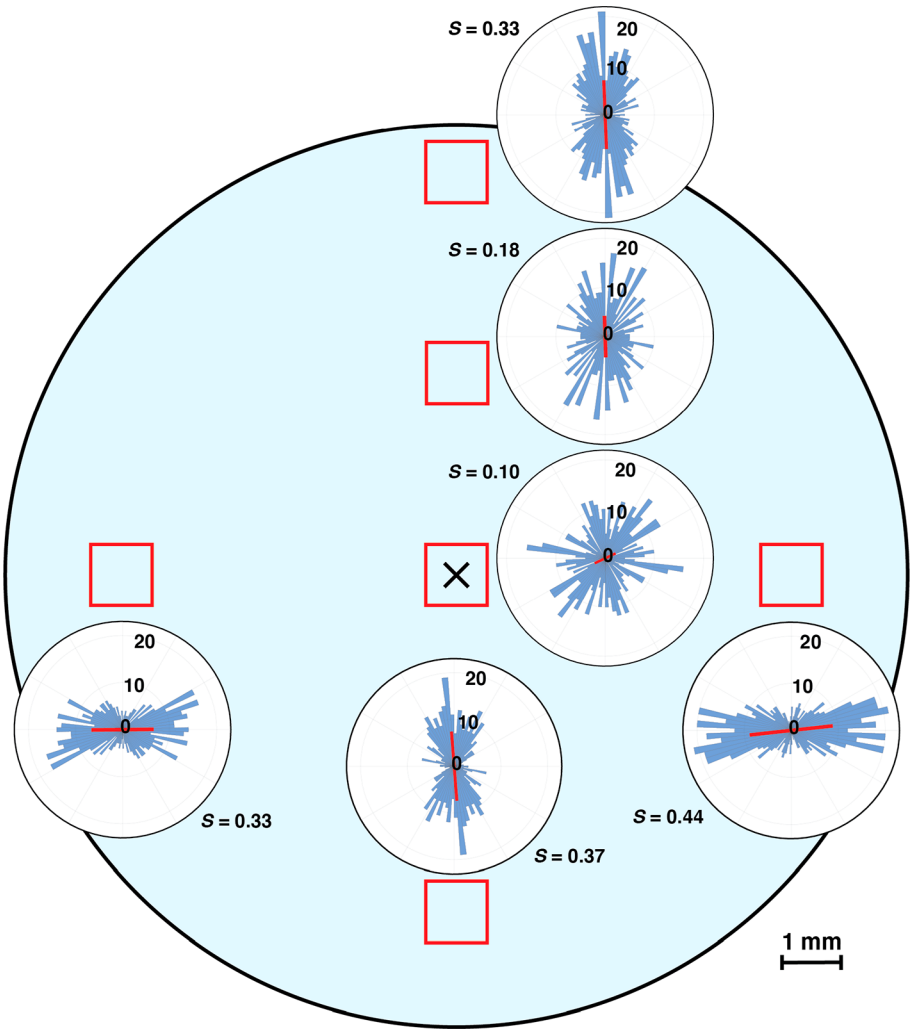

Figure 2. Polar histograms of the orientation of end-to-end vectors of chains imaged in the locations indicated by red boxes on the coverslip, which were 5 mm away from the center in the East, South, and West directions and 0, 3, and 6 mm away in the North direction. Ensembles are made up of 350 chains for each location. The order parameter S is indicated on the side of each of the polar histograms, and the red lines point in the direction of the average orientation, with the ratio of their length to the diameter of the histogram indicating the value of S. The East, South, and West locations are imaged from the same film, and a location in the North direction 5 mm away from the center on this film had $S = 0.43$, not shown in this figure. The shown North locations at 3 and 6 mm are imaged from a different film.

that no anisotropy is present. This is done by first determining the 2D order parameter S given by

$$S = \langle 2\cos^2\theta - 1 \rangle \quad (1)$$

where θ is the difference between the angle of each chain and the average angle of the entire ensemble. A value of $S = 0$ indicates randomly oriented chains, and $S = 1$ indicates all chains pointing in the same direction. For the ensemble of 1068 chains (Figure 1b), we calculated an order parameter of 0.32. The Rayleigh test statistic is given by

$$z = nS^2 \quad (2)$$

where n is the sample size. We can reject the null hypothesis with 99% confidence for $n > 1000$ when the test statistic is above a critical value, $z > 4.60$.[37] The statistic for this experiment was $z = 110$, confirming significant orientation caused by shear forces on bottlebrushes in the polymer film.

To further test the effect of shear flow on orientation, we captured super-resolution images at various positions on the same sample (Figure 2). Moving between four different locations (North, East, South, West) relative to the center of the coverslip, we find the chains are generally oriented pointing toward the center, with similar order parameter values for similar distances from the center. Additionally, the order parameter increases from an insignificant value at the center to $S = 0.3$–0.4 at a distance of 5–6 mm away. These highly predictable and systematic results further confirm the significance of the preferential orientation phenomena.

The position-dependent orientation results are consistent with flow-induced alignment during the spin-coating process. In the commonly accepted model for spin-coating, after the liquid is applied, a solid film is formed after undergoing two successive phases.[38−41] (1) The first phase is dominated by outward flow of the liquid solution driven by centrifugal forces. (2) After the liquid film has thinned such that the velocities are negligible due to the no-slip condition at the substrate, evaporation of the solvent then dominates. During Phase 1, a simple solution of the Navier−Stokes equations (assuming a Newtonian fluid) with the lubrication approximation provides an expression for the shear rate, which is dominated by the radial component of the velocity

https://doi.org/10.1021/acs.nanolett.2c01830
Nano Lett. XXXX, XXX, XXX−XXX

$$\dot{\gamma}_{rz} = \frac{\partial v_r}{\partial z} = \frac{\rho \omega^2 r}{\mu}(h - z) \quad (3)$$

where ρ is the fluid density, μ is the viscosity, ω is the angular velocity of spin-coating, h is the time-dependent fluid film thickness, r is the radial distance from the center axis of rotation, and z is the distance from the surface of the coverslip (see Supporting Information for derivation). The maximum shear rate in the fluid with the density and viscosity of toluene at a position of r = 6 mm when the fluid layer is h = 100 μm thick is 1.26 × 10^5 s^{-1}. (h varies throughout Phase 1, but this value was chosen for demonstrative purposes, near the beginning of the coating process.) The rotational diffusivity of similarly sized colloidal rods of ∼300 nm has been measured to be $D_r \approx 10^1$ s^{-1}.[34] To describe the competing effects of hydrodynamics, which align the polymers, versus diffusion, which randomizes their orientation, the resulting Peclet number is $Pe = \dot{\gamma}/D_r \approx 10^4$, which is consistent with the results in Figure 2. We note that rotational diffusivity is only one mechanism that randomizes orientation, and other mechanisms such as chain relaxation could play a role. Eq 3 also explains the increasing S with distance from the center, as the shear rate increases linearly with radius. The S values significantly less than unity may be partially explained by the nonuniform shear rate through the thickness of the fluid film, which increases from zero at the fluid−air interface to its maximum at the substrate. Our SMLM experiments image through the entire thickness.

The two-phase model of spin-coating also provides predictions associated with Phase 2, when solvent evaporation dominates. Here, the fluid flow is negligible (Pe = 0), so the bottlebrush orientations can randomize for a duration that depends on the evaporation rate of the solvent. To study this dependence, we tested the effect of solvents with varying volatilities while holding other parameters constant, such as film thickness, spin speed, etc. We note that changes in solvent will simultaneously introduce confounding variables such as density, viscosity, and inter- and intramolecular interactions, but we assume these effects are minor compared to the evaporation rate. Based on 350 chains for each condition, we observe a decrease in the order parameter S as the solvent boiling point increases and thus volatility decreases (Figure 3). This agrees with our expectation: if the solvent evaporates more slowly, the chains have more time to undergo relaxation and randomize their orientations.[1]

The present results can be contextualized alongside the mature field of single-polymer rheology, where typically large fluorescent biopolymers such as DNA or actin are visualized in real time in flow.[42−47] Our SMLM experiments offer the obvious advantage of higher spatial resolution, which directly enables exploration of more application-relevant materials[48] and particularly in bulk environments. Some drawbacks include a more complex flow field during spin-coating, compared to simple shear or extensional flows that are commonly generated using microfluidics in previous studies. Real-time dynamics are also a challenge, as our experiment can be considered a single-polymer rheology experiment frozen in time, though significant progress has been made in other SMLM studies of biological dynamics.[49] On the other hand, when compared to other techniques that measure orientation such as birefringence and P-RSoXS,[13−15] SMLM offers the key advantage of single-chain information. We can thus readily explore statistics beneath the ensemble, providing much more detailed information than just a bulk value of the order parameter. Two examples of this are shown below.

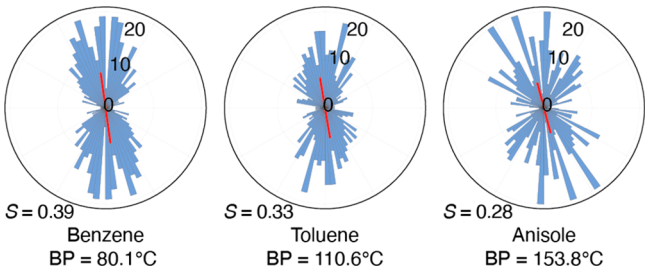

Figure 3. Polar histograms of the orientation of the end-to-end vectors in super-resolution images for samples spun using different solvents with boiling points (BPs). The order parameter is indicated, and the ratio of length of the red line to the diameter of each histogram reflects the magnitude of S. The images for each condition were taken 5 mm away from the center of the sample. Films (40 nm thick) were prepared by spin-coating each polymer solution at 3000 rpm.

One may intuitively postulate that chains oriented by shear forces will take a more rigid conformation. In fact, this result is demonstrated in other studies, which have directly observed the elongational effects of shear forces on polymer chains.[43,45,46] From our experiments, we may expect to find that chains oriented toward the direction of the centrifugal force have a higher apparent persistence length l_p due to the effects from shearing flow. Specifically, alignment of the chain over its length will cause the tangent−tangent correlation function to decay to a nonzero asymptotic value,[50] which would cause l_p to appear higher when fitting to a zero-asymptote exponential function, as we do. We thus revisit the 1068 chain ensemble from Figure 1 to directly study the effect of orientation and rigidity. Here, we take smaller subsets of chains binned by the direction of their end-to-end vectors and calculate a persistence length l_p based on the smaller ensemble for each direction. We plot the l_p vs the average angle of each bin in Figure 4. While the data does not show a strong

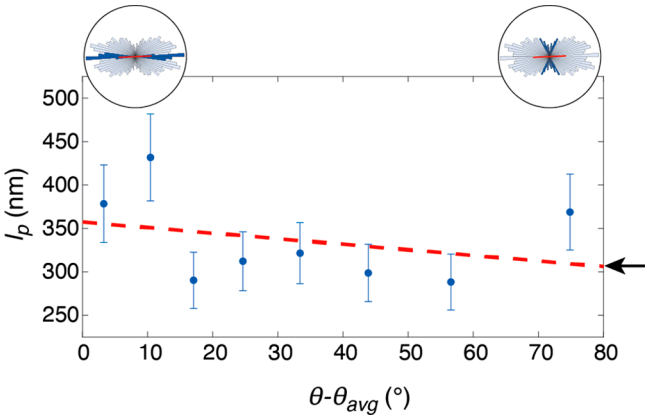

Figure 4. Plot of persistence length l_p vs average angle of each binned subset of the ensemble of chains in Figure 1B. Each point consists of 133 chains, and the spans of each bin are provided in Table S1. The 95% confidence intervals are calculated based on 7 sets of 133 wormlike chains from simulation. This analysis was performed in a previous study.[29] The red dashed line is a linear fit to the data, with R^2 = 0.091. The arrow indicates the postannealed persistence length of this polymer, which is 307 nm. The polar histograms display the bins of chains closest to (left) and farthest from (right) the average angle.

https://doi.org/10.1021/acs.nanolett.2c01830
Nano Lett. XXXX, XXX, XXX−XXX

relationship, a slight correlation is suggested where chains closer to the flow direction have a higher persistence length, which may be explained by the expected extensional effects from shear flow.

We further analyze the large ensemble to understand the effect of chain length on orientation. During the evaporation step, where flow is negligible and no longer affects the chains, we expect chains to begin to relax to their equilibrium isotropic conformations before becoming kinetically trapped when all the solvent has evaporated. Additionally, shorter chains have a higher rotational diffusivity D_r than longer chains and should thus relax faster. For example, for rigid rods in dilute solution, the dependence on contour length L is $D_r \approx L^{-3}$. Although our system is a concentrated solution of relatively rigid chains surrounded by flexible polymers, we can still expect a strong inverse relationship between D_r and L. We plot the order parameter S vs contour length L_0 (Figure 5). Each condition consists of 213 chains. Despite expecting longer chains to retain their orientation, our results show a slight trend that suggests the opposite result: the ensemble consisting of the longest chains has the lowest order parameter. While this seems to be a relatively weak dependence, we briefly speculate on its origin. During evaporation, we expect conformational relaxation to require mobility at the local scale and thus occurs faster than orientational relaxation toward isotropy. As chains approach their equilibrium conformations, longer chains will have a lower value of the tangent−tangent correlation function, which decays exponentially with distance. This results in the end-to-end vectors of longer chains pointing farther away from the shear direction. Rather than an effect of rotational diffusion, the decrease in S for longer chains is possibly an effect of chain relaxation.

In this work, we study shear effects on the chain orientation of bottlebrush polymers through direct imaging by SMLM. The direction of the end-to-end vectors of the chains is driven by the outward flow during spin-coating. We have captured direct evidence of these effects, displaying a strong dependence bof the direction and degree of orientation on the direction and magnitude of shear forces. Additionally, we tested the effects of evaporation rate, providing evidence of relaxation during the evaporation step of spin-coating. Investigation of the relationship between orientation and chain rigidity suggests some relationship, though the observed trend is not particularly strong. Finally, longer chains show a greater deviation from the ensemble-average direction. Ultimately, our access to location- and chain-specific information allows us to study orientation as it changes throughout the film and probe how various experimental conditions affect anisotropy.

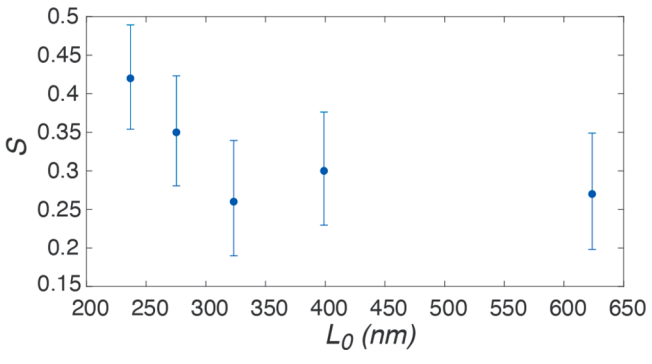

Figure 5. Order parameter S vs contour length L_0. Each data point is based on an ensemble of 5 equally binned sets of 213 chains and is based on the 1068 chain ensemble discussed previously (Figure 1B). L_0 was determined from the skeletonized traces extracted from our image analysis code. The error bars are 95% confidence intervals based on the simulated probability distribution of S over N = 213 chains, assuming each chain orientation follows the von Mises distribution.

EXPERIMENTAL METHODS

All materials were acquired from Sigma-Aldrich unless otherwise stated. Fluorescently labeled bottlebrush polymers were synthesized using previously published methods using a grafting-from approach.[51−53] Poly(2-hydroxyethyl methacrylate) (PolymerSource M_n = 410 000 g/mol, Đ = 1.55) was functionalized by coupling with α-bromoisobutyryl bromide to form poly(2-(2-bromoisobutyryloxy)ethyl methacrylate) (PBIEM). The identity of PBIEM was confirmed using ^{1}H NMR (Bruker Avance III HD 400 MHz system). Polymerization and successful dye attachment were confirmed using gel permeation chromatography (GPC) using a preparative-scale system (JAI LaboACE LC5060, Shodex KF-806L and KF-803L columns) equipped with a light scattering detector (Wyatt Dawn 8) operated with chloroform at 1 mL/min. The dn/dc value used for PMMA in chloroform was determined to be 0.065 mL/g. The side chain molecular weight was determined by cleaving the side chains from the backbone by methanolysis and characterized using the same preparative GPC as above.

Thin films were prepared by spin-coating solutions of linear PMMA (350 000 g/mol) with a dilute amount of dyed bottlebrush PMMA (0.03:1 dyed to undyed polymer by weight) from various solvents. Films were prepared at room temperature (20−22 °C), which varied only by a few degrees even though it was not precisely controlled. For toluene and anisole as the solvent, solution concentrations were 1 wt %, while 0.5 wt % was used for benzene, all to achieve the same film thickness. These concentrations are very dilute and thus far below the overlap concentration c^*. Most of the films were prepared using toluene, unless otherwise indicated, and spun at 3000 rpm on #1.5 glass coverslips, which underwent Piranha treatment (1:3, 30% H_2O_2 solution to H_2SO_4) for at least 3 h. Polymer films were measured to be approximately 40 nm thick by ellipsometry (J.A. Wollam Co., M-2000D).

Polymer films were imaged using previously published methods.[29,52] An identical optical setup was also used, which featured a custom modified Olympus IX73 inverted microscope equipped with optical components from ThorLabs. From super-resolution images, bottlebrush polymers were chosen based on size (>250 nm) and shape (elongated). These images were skeletonized, tracing a line through the center of each feature using an image processing code written in MATLAB. The end-to-end vector was extracted from these skeletonized traces by taking the difference between the end points of the trace. From the ensemble of calculated angles, we calculated the circular mean using the equation

$$\theta_{avg} = a\tan 2\left(\sum_{i=1}^{n} \sin\theta_i, \sum_{i=1}^{n} \cos\theta_i\right)$$

where n is the number of chains, doubling the angle values to account for the bidirectionality. Because the calculated angles range from −90 to +90°, when plotting the polar histograms, we plotted θ and θ + 180° to reflect the bidirectional nature of

https://doi.org/10.1021/acs.nanolett.2c01830
Nano Lett. XXXX, XXX, XXX−XXX

the end-to-end vectors, resulting in symmetric histograms. Persistence lengths were determined by exponential fits to the tangent−tangent correlation function, as described in a previous study.[29]

■ ASSOCIATED CONTENT

Supporting Information

The Supporting Information is available free of charge at https://pubs.acs.org/doi/10.1021/acs.nanolett.2c01830.

Additional methods, materials, and figures including ^{1}H NMR, gel permeation chromatography, effects of thermal annealing, derivation of the expression of shear rate, and bin locations for angle and contour length studies (PDF)

■ AUTHOR INFORMATION

Corresponding Author

Muzhou Wang − *Department of Chemical and Biological Engineering, Northwestern University, Evanston, Illinois 60208, United States;* orcid.org/0000-0002-7054-3022; Email: mwang@northwestern.edu

Author

Jonathan M. Chan − *Department of Chemical and Biological Engineering, Northwestern University, Evanston, Illinois 60208, United States*

Complete contact information is available at: https://pubs.acs.org/10.1021/acs.nanolett.2c01830

Notes

The authors declare no competing financial interest.

■ ACKNOWLEDGMENTS

The authors acknowledge Profs. Wesley Burghardt, Julia Kalow, and John Torkelson for access to equipment and useful discussions. We also acknowledge funding from the American Chemical Society Petroleum Research Fund and the National Science Foundation (DMR-1945249) for support of this work. This work made use of the Integrated Molecular Structure Education and Research Center (IMSERC) facility at Northwestern University, which has received support from the Soft and Hybrid Nanotechnology Experimental Resource (NSF ECCS-2025633), the State of Illinois, and the International Institute for Nanotechnology.

■ REFERENCES

(1) DeLongchamp, D. M.; Vogel, B. M.; Jung, Y.; Gurau, M. C.; Richter, C. A.; Kirillov, O. A.; Obrzut, J.; Fischer, D. A.; Sambasivan, S.; Richter, L. J.; Lin, E. K. Variations in Semiconducting Polymer Microstructure and Hole Mobility with Spin-Coating Speed. *Chem. Mater.* **2005**, *17* (23), 5610−5612.

(2) Kinder, L.; Kanicki, J.; Petroff, P. Structural Ordering and Enhanced Carrier Mobility in Organic Polymer Thin Film Transistors. *Synth. Met.* **2004**, *146* (2), 181−185.

(3) Müller, C.; Aghamohammadi, M.; Himmelberger, S.; Sonar, P.; Garriga, M.; Salleo, A.; Campoy-Quiles, M. One-Step Macroscopic Alignment of Conjugated Polymer Systems by Epitaxial Crystallization during Spin-Coating. *Adv. Funct. Mater.* **2013**, *23* (19), 2368−2377.

(4) Bao, Z. Materials and Fabrication Needs for Low-Cost Organic Transistor Circuits. *Adv. Mater.* **2000**, *12* (3), 227−230.

(5) Hiszpanski, A. M.; Baur, R. M.; Kim, B.; Tremblay, N. J.; Nuckolls, C.; Woll, A. R.; Loo, Y. L. Tuning Polymorphism and Orientation in Organic Semiconductor Thin Films via Post-Deposition Processing. *J. Am. Chem. Soc.* **2014**, *136* (44), 15749−15756.

(6) Gargi, D.; Kline, R. J.; Delongchamp, D. M.; Fischer, D. A.; Toney, M. F.; O'Connor, B. T. Charge Transport in Highly Face-On Poly(3-Hexylthiophene) Films. *J. Phys. Chem. C* **2013**, *117* (34), 17421−17428.

(7) Ward, I. M. Mechanical Properties of Oriented Polymers. *Polymer* **1974**, *15* (6), 379−386.

(8) Yu, L.; Christie, G. Microstructure and Mechanical Properties of Orientated Thermoplastic Starches. *J. Mater. Sci.* **2005**, *40* (1), 111−116.

(9) Wang, Z. H.; Chen, X.; Yang, H. X.; Zhao, J.; Yang, S. Y. The In-Plane Orientation and Thermal Mechanical Properties of the Chemically Imidized Polyimide Films. *Chin. J. Polym. Sci. (English Ed.* **2019**, *37* (3), 268−278.

(10) Guo, Y.; Ruan, K.; Shi, X.; Yang, X.; Gu, J. Factors Affecting Thermal Conductivities of the Polymers and Polymer Composites: A Review. *Compos. Sci. Technol.* **2020**, *193* (March), 108134.

(11) Chen, H.; Ginzburg, V. V.; Yang, J.; Yang, Y.; Liu, W.; Huang, Y.; Du, L.; Chen, B. Thermal Conductivity of Polymer-Based Composites: Fundamentals and Applications. *Prog. Polym. Sci.* **2016**, *59*, 41−85.

(12) Kaito, A.; Kyotani, M.; Nakayama, K. Orientation Profiles in the Strand of Thermotropic Liquid-Crystalline Polymer Studied by Polarized Fourier Transform Infrared Microspectroscopy. *Macromolecules* **1991**, *24* (11), 3244−3249.

(13) Frka-Petesic, B.; Sugiyama, J.; Kimura, S.; Chanzy, H.; Maret, G. Negative Diamagnetic Anisotropy and Birefringence of Cellulose Nanocrystals. *Macromolecules* **2015**, *48* (24), 8844−8857.

(14) Maret, G.; Weill, G. Magnetic Birefringence Study of the Electrostatic and Intrinsic Persistence Length of DNA. *Biopolymers* **1983**, *22* (12), 2727−2744.

(15) Litofsky, J. H.; Lee, Y.; Aplan, M. P.; Kuei, B.; Hexemer, A.; Wang, C.; Wang, Q.; Gomez, E. D. Polarized Soft X-Ray Scattering Reveals Chain Orientation within Nanoscale Polymer Domains. *Macromolecules* **2019**, *52* (7), 2803−2813.

(16) Mukherjee, S.; Streit, J. K.; Gann, E.; Saurabh, K.; Sunday, D. F.; Krishnamurthy, A.; Ganapathysubramanian, B.; Richter, L. J.; Vaia, R. A.; DeLongchamp, D. M. Polarized X-Ray Scattering Measures Molecular Orientation in Polymer-Grafted Nanoparticles. *Nat. Commun.* **2021**, *12* (1), 4896.

(17) Predecki, P.; Statton, W. O. Dislocations Caused by Chain Ends in Crystalline Polymers. *J. Appl. Phys.* **1966**, *37* (11), 4053−4059.

(18) Lee, S.; Pharr, M. Sideways and Stable Crack Propagation in a Silicone Elastomer. *Proc. Natl. Acad. Sci. U. S. A.* **2019**, *116* (19), 9251−9256.

(19) Stephen, M. J.; Straley, J. P. Physics of Liquid Crystals. *Rev. Mod. Phys.* **1974**, *46* (4), 617−704.

(20) Sun, G.; Cho, S.; Clark, C.; Verkhoturov, S. V.; Eller, M. J.; Li, A.; Pavía-Jiménez, A.; Schweikert, E. A.; Thackeray, J. W.; Trefonas, P.; Wooley, K. L. Nanoscopic Cylindrical Dual Concentric and Lengthwise Block Brush Terpolymers as Covalent Preassembled High-Resolution and High-Sensitivity Negative-Tone Photoresist Materials. *J. Am. Chem. Soc.* **2013**, *135* (11), 4203−4206.

(21) Patel, B.; Walsh, D.; Patel, K.; Kim, D. H.; Kwok, J.; Guironnet, D.; Diao, Y. Rapid, Interface-Driven Domain Orientation in Bottlebrush Diblock Copolymer Films During Thermal Annealing. *Soft Matter* **2022**, *18*, 1666.

(22) Yavitt, B. M.; Gai, Y.; Song, D. P.; Winter, H. H.; Watkins, J. J. High Molecular Mobility and Viscoelasticity of Microphase-Separated Bottlebrush Diblock Copolymer Melts. *Macromolecules* **2017**, *50* (1), 396−405.

(23) Sveinbjornsson, B. R.; Weitekamp, R. A.; Miyake, G. M.; Xia, Y.; Atwater, H. A.; Grubbs, R. H. Rapid Self-Assembly of Brush Block Copolymers to Photonic Crystals. *Proc. Natl. Acad. Sci. U. S. A.* **2012**, *109* (36), 14332−14336.

(24) Cheng, L. C.; Gadelrab, K. R.; Kawamoto, K.; Yager, K. G.; Johnson, J. A.; Alexander-Katz, A.; Ross, C. A. Templated Self-

Assembly of a PS- Branch-PDMS Bottlebrush Copolymer. *Nano Lett.* **2018**, *18* (7), 4360−4369.
(25) Sunday, D. F.; Chang, A. B.; Liman, C. D.; Gann, E.; Delongchamp, D. M.; Thomsen, L.; Matsen, M. W.; Grubbs, R. H.; Soles, C. L. Self-Assembly of ABC Bottlebrush Triblock Terpolymers with Evidence for Looped Backbone Conformations. *Macromolecules* **2018**, *51* (18), 7178−7185.
(26) Dalsin, S. J.; Rions-Maehren, T. G.; Beam, M. D.; Bates, F. S.; Hillmyer, M. A.; Matsen, M. W. Bottlebrush Block Polmers: Quantitative Theory and Experiments. *ACS Nano* **2015**, *9* (12), 12233−12245.
(27) Qiang, Z.; Wang, M. 100th Anniversary of Macromolecular Science Viewpoint: Enabling Advances in Fluorescence Microscopy Techniques. *ACS Macro Lett.* **2020**, *9* (9), 1342−1356.
(28) Thompson, M. A.; Lew, M. D.; Moerner, W. E. Extending Microscopic Resolution with Single-Molecule Imaging and Active Control. *Annu. Rev. Biophys.* **2012**, *41* (1), 321−342.
(29) Chan, J. M.; Kordon, A. C.; Zhang, R.; Wang, M. Direct Visualization of Bottlebrush Polymer Conformations in the Solid State. *Proc. Natl. Acad. Sci. U. S. A.* **2021**, *118* (40), e2109534118.
(30) Wade, M. A.; Walsh, D.; Lee, J. C. W.; Kelley, E.; Weigandt, K.; Guironnet, D.; Rogers, S. A. Color, Structure, and Rheology of a Diblock Bottlebrush Copolymer Solution. *Soft Matter* **2020**, *16* (21), 4919−4931.
(31) Dalsin, S. J.; Hillmyer, M. A.; Bates, F. S. Molecular Weight Dependence of Zero-Shear Viscosity in Atactic Polypropylene Bottlebrush Polymers. *ACS Macro Lett.* **2014**, *3* (5), 423−427.
(32) Patel, B. B.; Walsh, D. J.; Kim, D. H.; Kwok, J.; Lee, B.; Guironnet, D.; Diao, Y. Tunable Structural Color of Bottlebrush Block Copolymers through Direct-Write 3D Printing from Solution. *Sci. Adv.* **2020**, *6* (24), eaaz7202.
(33) López-Barrón, C. R.; Shivokhin, M. E. Extensional Strain Hardening in Highly Entangled Molecular Bottlebrushes. *Phys. Rev. Lett.* **2019**, *122* (3), 37801.
(34) Calabrese, V.; Haward, S. J.; Shen, A. Q. Effects of Shearing and Extensional Flows on the Alignment of Colloidal Rods. *Macromolecules* **2021**, *54* (9), 4176−4185.
(35) Allen, R.; Bao, Z.; Fuller, G. G. Oriented, Polymer-Stabilized Carbon Nanotube Films: Influence of Dispersion Rheology. *Nanotechnology* **2013**, *24* (1), 015709.
(36) Geng, Y.; Dalhaimer, P.; Cai, S.; Tsai, R.; Tewari, M.; Minko, T.; Discher, D. E. Shape Effects of Filaments versus Spherical Particles in Flow and Drug Delivery. *Nat. Nanotechnol.* **2007**, *2* (4), 249−255.
(37) Fisher, N. I. *Statistical Analysis of Circular Data*; Cambridge University Press, 1993.
(38) Mouhamad, Y.; Mokarian-Tabari, P.; Clarke, N.; Jones, R. A. L.; Geoghegan, M. Dynamics of Polymer Film Formation during Spin Coating. *J. Appl. Phys.* **2014**, *116* (12), 123513.
(39) Tyona, M. D. A Theoritical Study on Spin Coating Technique. *Adv. Mater. Res.* **2013**, *2* (4), 195−208.
(40) Lawrence, C. J. The Mechanics of Spin Coating of Polymer Films. *Phys. Fluids* **1988**, *31* (10), 2786−2795.
(41) Hall, D. B.; Underhill, P.; Torkelson, J. M. Spin Coating of Thin and Ultrathin Polymer. *Polym. Eng. Sci.* **1998**, *38* (12), 2039−2045.
(42) Mai, D. J.; Schroeder, C. M. 100th Anniversary of Macromolecular Science Viewpoint: Single-Molecule Studies of Synthetic Polymers. *ACS Macro Lett.* **2020**, *9* (9), 1332−1341.
(43) Mai, D. J.; Saadat, A.; Khomami, B.; Schroeder, C. M. Stretching Dynamics of Single Comb Polymers in Extensional Flow. *Macromolecules* **2018**, *51* (4), 1507−1517.
(44) Abadi, M.; Serag, M. F.; Habuchi, S. Entangled Polymer Dynamics beyond Reptation. *Nat. Commun.* **2018**, *9* (1), 5098.
(45) Smith, D. E.; Babcock, H. P.; Chu, S. Single-Polymer Dynamics in Steady Shear Flow. *Science* **1999**, *283* (5408), 1724−1727.
(46) Gerashchenko, S.; Chevallard, C.; Steinberg, V. Single-Polymer Dynamics: Coil-Stretch Transition in a Random Flow. *Europhys. Lett.* **2005**, *71* (2), 221−227.
(47) Käs, J.; Strey, H.; Sackmann, E. Direct Imaging of Reptation for Semiflexible Actin Filaments. *Nature* **1994**, *368* (6468), 226−229.
(48) Schroeder, C. M. Single Polymer Dynamics for Molecular Rheology. *J. Rheol.* **2018**, *62* (1), 371−403.
(49) Huang, F.; Hartwich, T. M. P.; Rivera-Molina, F. E.; Lin, Y.; Duim, W. C.; Long, J. J.; Uchil, P. D.; Myers, J. R.; Baird, M. A.; Mothes, W.; Davidson, M. W.; Toomre, D.; Bewersdorf, J. Video-Rate Nanoscopy Using SCMOS Camera-Specific Single-Molecule Localization Algorithms. *Nat. Methods* **2013**, *10* (7), 653−658.
(50) Köster, S.; Steinhauser, D.; Pfohl, T. Brownian Motion of Actin Filaments in Confining Microchannels. *J. Phys.: Condens. Matter* **2005**, *17* (49), S4091−S4104.
(51) Rzayev, J. Synthesis of Polystyrene-Polylactide Bottlebrush Block Copolymers and Their Melt Self-Assembly into Large Domain Nanostructures. *Macromolecules* **2009**, *42* (6), 2135−2141.
(52) Qiang, Z.; Shebek, K. M.; Irie, M.; Wang, M. A Polymerizable Photoswitchable Fluorophore for Super-Resolution Imaging of Polymer Self-Assembly and Dynamics. *ACS Macro Lett.* **2018**, *7* (12), 1432−1437.
(53) Uno, K.; Niikura, H.; Morimoto, M.; Ishibashi, Y.; Miyasaka, H.; Irie, M. In Situ Preparation of Highly Fluorescent Dyes upon Photoirradiation. *J. Am. Chem. Soc.* **2011**, *133* (34), 13558−13564.

https://doi.org/10.1021/acs.nanolett.2c01830
Nano Lett. XXXX, XXX, XXX−XXX